Geochemistry Geophysics Geosystems G3
AN ELECTRONIC JOURNAL OF THE EARTH SCIENCES
Published by AGU and the Geochemical Society

Article
Volume 9, Number 2
22 February 2008
Q02014, doi:10.1029/2007GC001776
ISSN: 1525-2027

Slab stiffness control of trench motion: Insights from numerical models

E. Di Giuseppe
Institute of Geophysics, ETH Zurich, Campus Hoenggerberg, Schaffmattstr. 30, CH-8093 Zurich, Switzerland (erika.digiuseppe@tomo.ig.erdw.ethz.ch)

Dipartimento di Scienze Geologiche, Università degli Studi "Roma Tre," L.go S. Leonardo Murialdo, I-00146, Rome, Italy

J. van Hunen
Department of Earth Sciences, Durham University, Durham DH1 3LE, UK (jeroen.van-hunen@durham.ac.uk)

F. Funiciello and C. Faccenna
Dipartimento di Scienze Geologiche, Università degli Studi "Roma Tre," L.go S. Leonardo Murialdo, I-00146, Rome, Italy (ffunicie@uniroma3.it; faccenna@uniroma3.it)

D. Giardini
Institute of Geophysics, ETH Zurich, Campus Hoenggerberg, Schaffmattstr. 30, CH-8093 Zurich, Switzerland (d.giardini@sed.ethz.ch)

[1] Subduction zones are not static features, but trenches retreat (roll back) or advance. Here, we investigate the dominant dynamic controls on trench migration by means of two- and three-dimensional numerical modeling of subduction. This investigation has been carried out by systematically varying the geometrical and rheological model parameters. Our viscoplastic models illustrate that advancing style subduction is promoted by a thick plate, a large viscosity ratio between plate and mantle, and a small density contrast between plate and mantle or an intermediate width ($w \sim 1300$ km). Advancing slabs dissipate ~45% to ~50% of the energy in the system. Thin plates with relatively low viscosity or relatively high density, or wide slabs (w ~ 2300 km), on the other hand, promote subduction in the retreating style (i.e., slab roll-back). The energy dissipated by a retreating slab is ~35% to ~40% of the total dissipated energy. Most of the energy dissipation occurs in the mantle to accommodate the slab motion, whereas the lithosphere dissipates the remaining part to bend and "unbend." With a simple scaling law we illustrate that this complex combination of model parameters influencing trench migration can be reduced to a single one: plate stiffness. Stiffer slabs cause the trench to advance, whereas more flexible slabs lead to trench retreat. The reason for this is that all slabs will bend into the subduction zone because of their low plastic strength near the surface, but stiff slabs have more difficulty "unbending" at depth, when arriving at the 660-km discontinuity. Those bent slabs tend to cause the trench to advance. In a similar way, variation of the viscoplasticity parameters in the plate may change the style of subduction: a low value of friction coefficient weakens the plate and results in a retreating style, while higher values strengthen the plate and promote the advancing subduction style. Given the fact that also on Earth the oldest (and therefore probably stiffest) plates have the fastest advancing trenches, we hypothesize that the ability of slabs to unbend after subduction forms the dominant control on trench migration.

Components: 10,327 words, 12 figures, 2 tables.

Keywords: subduction; numerical models; trench motion.

Index Terms: 8120 Tectonophysics: Dynamics of lithosphere and mantle: general (1213); 8170 Tectonophysics: Subduction zone processes (1031, 3060, 3613, 8413); 8149 Tectonophysics: Planetary tectonics (5475).

Received 10 August 2007; **Revised** 25 October 2007; **Accepted** 7 November 2007; **Published** 22 February 2008.

Di Giuseppe, E., J. van Hunen, F. Funiciello, C. Faccenna, and D. Giardini (2008), Slab stiffness control of trench motion: Insights from numerical models, *Geochem. Geophys. Geosyst.*, *9*, Q02014, doi:10.1029/2007GC001776.

1. Introduction

[2] Subduction operates by bending of the lithospheric plate at the trench. The geometries of a bending slab indicate significant deformation, suggesting that lithospheric plates might be weakened somehow during subduction [*Tao and O'Connell*, 1993]. Detailed seismic images on the oceanic trench slope offshore of Middle America and Chile subduction zones show that faults down to lower crustal depth accommodate bending [*Ranero et al.*, 2003; *Grevemeyer et al.*, 2005], promoting hydration of the crust and weakening the lithospheric strength by possible serpentinization. The presence of near trench volcanism and massive brittle deformation in the forebulge area are other independent key observations that lithosphere can substantially break and weaken before entering at trench [*Hirano et al.*, 2006; *Billi et al.*, 2006].

[3] The slab strength at the trench has important consequences for the kinematics of the subduction process as well. Dynamically self-consistent numerical [*Gurnis and Hager*, 1988; *Zhong and Gurnis*, 1995; *Funiciello et al.*, 2003a; *Enns et al.*, 2005; *Stegman et al.*, 2006] and laboratory models [*Funiciello et al.*, 2003b; *Bellahsen et al.*, 2005; *Faccenna et al.*, 2007] show that the slab strength play a key role in controlling subduction velocity and its partitioning between trench and plate motion. *Bellahsen et al.* [2005] highlight for the first time that the "free" subduction occurs with two main styles: an advancing and a retreating one. *Faccenna et al.* [2007] show that the style of subduction at steady state mainly depends on the resistance encountered by the slab to bend and penetrate into the upper mantle. Despite the many studies to the lithospheric strength and its weakening caused by the yield stress [e.g., *Martinod and Molnar*, 1995; *Kohlstedt et al.*, 1995], the bending mechanism in the subduction process is still poorly constrained. Simple calculations indeed show that the bending stress at the trench (either for viscous or viscoelastic plates [see *Turcotte and Schubert*, 1982]) exceeds the total strength of the lithosphere itself [*Bodine et al.*, 1981; *Conrad and Hager*, 1999]. The reduction in plate strength is consistent with several geodynamical models that use different rheologies: viscous models [*Zhong and Gurnis*, 1994] in which the plate boundaries are modeled as faults, and elastic [*Caldwell et al.*, 1976], elastoplastic [*Turcotte et al.*, 1978], or viscoelastic models [*Bott*, 1993].

[4] On Earth such a partition of the subduction zones between retreating and advancing styles can be recognized in different geographical reference frames, as illustrated by F. Funiciello et al. (Trench migration, net rotation and slab-mantle coupling, submitted to *Earth and Planetary Science Letters*, 2007; hereinafter referred to as Funiciello et al., submitted manuscript, 2007) and *Heuret* [2005]. In our models we obtain both subduction modes with a realistic range of geometrical and rheological parameter settings.

[5] With purely viscous analogue models, *Bellahsen et al.* [2005] carried out a systematical dynamics study on the effects of the rheological and geometrical parameters on the subduction style. They found that denser, thinner and/or larger plates favor trench retreat, while less dense, thicker and narrower slabs promote advancing style subduction. *Schellart et al.* [2007] conducted 3-D numerical experiments, in which they investigated the effects of the slab width on the evolution of the subduction process. In their models, narrower slabs retreat fast ($w < 1000$ km), intermediate plates ($w \sim 2000$–3000 km) fold on the discontinuity, and wide ones ($w > 4000$ km) are almost stationary.

[6] In this work we describe the results of two-dimensional (2-D) and three-dimensional (3-D) numerical models that explore systematically how geometrical and rheological parameters affect the

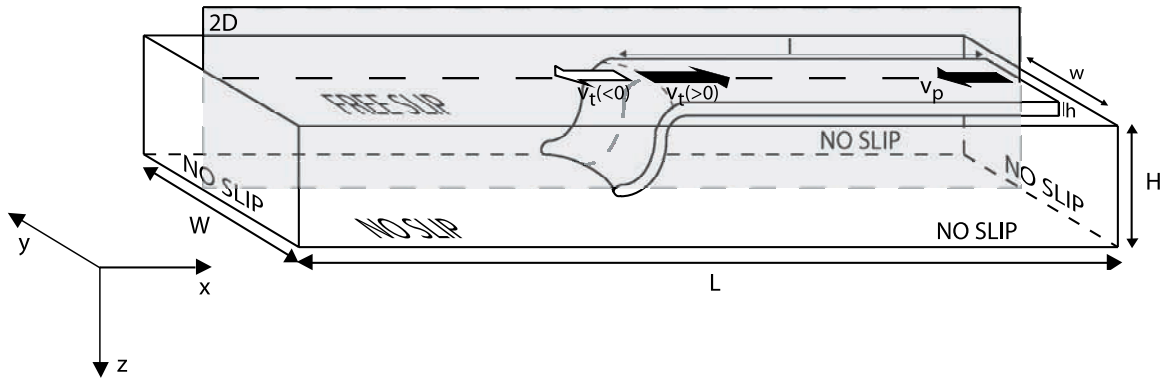

Figure 1. Three-dimensional numerical model setup describing a free slab sinking within the upper mantle, with the boundary conditions at top, bottom, and sides of the computational system. The 2-D setup is given by the vertical grey surface cross section. Arrows describe the trench motion, V_t, and the plate motion, V_p. Black and white arrows refer to positive and negative velocities, respectively.

kinematical/dynamic evolution of the subduction process. A viscoplastic rheology with a depth-dependent yield strength provides the rheological framework for the detachment of a plate from the surface and subsequent self-consistent sinking within the mantle. Those calculations illustrate that the style of subduction is governed by a combination of several physical parameters. By means of a scaling law, we are able to reduce the complexity of the system, and to identify lithospheric stiffness as the key parameter in the subduction process.

2. Model Setup

2.1. Governing Equations

[7] Subduction is modeled with a 2-D and 3-D setup for viscoplastic flow with compositional buoyancy (see Figure 1).

[8] The mantle is treated as an incompressible viscous medium, with an infinite Prandtl number and Boussinesq approximations. The system is described by the conservation of mass,

$$\nabla \cdot \vec{v} = 0 \tag{1}$$

momentum,

$$-\nabla\tau + \nabla p = \Delta\rho g\hat{z} \tag{2}$$

and chemical advection:

$$\frac{\partial C_o}{\partial t} + \left(\vec{v} \cdot \nabla\right) C_o = 0 \tag{3}$$

where $\vec{v}$ is the velocity vector, τ the deviatoric stress tensor, p the dynamic pressure, C_o the composition, and g the gravitational acceleration. The composition function C_o is a switch between two end-member components representative of the oceanic lithosphere and the upper mantle, respectively.

[9] Temperature is not explicitly solved and, consequently, thermal effects and phase changes are neglected. Instead, a compositional density contrast $\Delta\rho$ is imposed between the slab and the surrounding mantle. Such simplification, although numerically more challenging, provides an efficient means to supply insightful information about the influence of variations in plate thickness and width, or viscosity or density contrasts between slab and mantle on the dynamics of the subduction process, irrespective of the underlying often complex sources of those variations.

2.2. Model Rheology

[10] Earth's rheology is not uniform but strongly changes with depth. Pressure and temperature are not the only parameters that influence the strength of a rock. Also the presence of water and the applied stress have an important effect in deformation. The use of experimentally determined diffusion or dislocation creep flow laws leads to an effective viscosity that is much larger than observed in nature [*Kohlstedt et al.*, 1995]. The uppermost part of the lithosphere deforms in a brittle way following the relation:

$$\tau_{yield} = \mu_f \rho g z \tag{4}$$

where μ_f is the coefficient of internal friction and C_f is the frictional cohesive strength in the limit of zero hydrostatic pressure. This is derived from the empirical Byerlee's frictional law [*Byerlee*, 1968],

which describes material yielding when normal stresses reach a critical value:

$$\tau_{yield} = C_f + \mu_f \sigma_n \quad (5)$$

[11] In this work, we model the yield criterion by assuming C_f to be equal zero and the normal stress σ_n to be the lithostatic pressure [*Moresi and Solomatov*, 1998; *van Hunen et al.*, 2001; *Enns et al.*, 2005; *Stegman et al.*, 2006]. However, the effective stress can be rewritten in the following terms [*Huismans et al.*, 2005]:

$$\tau_{yield} = P^* \sin(\alpha) \quad (6)$$

where α is the angle of internal friction, and P can be taken equal to ρgz. Since, the coefficient of friction is:

$$\mu_f = \tan(\alpha) \quad (7)$$

and the angle α is small, it is possible to approximate $\tan(\alpha) \sim \sin(\alpha)$ and equations (4) and (6) are equivalent.

2.3. Numerical Method

[12] Two-dimensional and three-dimensional calculations are performed using the parallel finite element (FE) code Citcom [*Moresi and Solomatov*, 1995; *Moresi and Gurnis*, 1996; *Zhong et al.*, 2000]. The governing equations are solved using an iterative conjugate gradient solver on an orthogonal mesh. Compositional information is carried by a large number of particles, more than hundred tracers per finite element in order to ensure enough numerical accuracy. Tracers are transported with the velocity field [e.g., *van Hunen et al.*, 2002] by applying a second-order Runge-Kutta method. The code is benchmarked against *van Keken et al.* [1997]. The second-order Runge-Kutta time stepping is accurate enough for these rather short trajectories.

[13] The computational domain is a 3-D Cartesian box of 4620 km long, 4620 km wide and 660 km deep (aspect ratio $7 \times 7 \times 1$) with 32 elements in vertical direction and 192 in both horizontal directions. The 2-D box has the same x and z dimensions and 64 and 384 elements in vertical and horizontal direction, respectively. In the 3-D case the resolution is lowered because the models are computationally more demanding. We tested that resolution changes did not affect the dynamics of the system but only the quality of visualization.

[14] The model consists of a compositionally described plate on top of a less viscous upper mantle (Figure 1). This setup is inspired by *Bellahsen et al.* [2005], and has the following characteristics:

[15] 1. No external forces are imposed to the system. Gravity drives the process entirely.

[16] 2. The trailing edge of the plate is detached from the side boundary, corresponding to zero ridge resistance (in the sense of *Kincaid and Olson* [1987]). We refer to this situation as a "free ridge" condition on the trailing edge of the subducting plate.

[17] 3. Subduction is triggered by an initial asymmetrical configuration of the slab: the leading edge of the slab has been curved into the mantle to induce a finite-amplitude instability after which the subduction process begins.

[18] 4. We use a passively convecting mantle. Hence, in our experiments only the subduction process, and no background convection or local background flow, generates mantle flow.

[19] 5. The oceanic lithosphere and upper mantle respect the range of natural density and viscosity contrasts [*Hager*, 1984; *Davies and Richards*, 1992; *Mitrovica and Forte*, 1997; *Vassiliou et al.*, 1984; *Vassiliou and Hager*, 1988; *Cloos*, 1993]. Its effective viscosity is temperature- and pressure-independent, but is strongly non-linear close to the surface.

[20] 6. The overriding plate is not modeled. We simplified the subduction zone by assuming that plates are surrounded by weak zones, whose viscosity is the same as the upper mantle [*King and Hager*, 1990]. In this way the "plate-like" behavior is preserved and the mobility of the plate is guaranteed. This setup conforms to the assumption of negligible interaction with external forces including those with an overriding plate. Obviously, interaction with the back-arc and mantle wedge, however important [*Billen and Gurnis*, 2001; *van Keken*, 2003], are affected by this measure.

[21] 7. The boundary conditions are described by a free-slip top and by no-slip bottom and sidewalls conform Bellahsen's laboratory models. The bottom boundary, associated with the 660-km discontinuity, is simulated as an impermeable barrier to flow, even though natural slabs are known to be able to penetrate into the lower mantle [*Fukao et al.*, 2001]. This impermeability assumption is motivated by the fact that the upper-lower mantle transition zone is related to an endothermic phase

change [*Ringwood and Irifune*, 1988] generating buoyancy forces that keep the slab (at least temporarily) from directly penetrating into the lower mantle [*Griffiths and Turner*, 1988; *Davies*, 1995; *Funiciello et al.*, 2004].

2.4. Output Data

[22] Each model is monitored geometrically (slab shape), kinematically (trench, plate, and subduction velocity) and dynamically (energy dissipation) throughout the subduction process. The position of trench and plate at different time steps are tracked throughout the calculation. Hence the plate velocity V_p and trench velocity V_t are calculated as the difference in position between a numerical time step and the previous one divided by the incremental time step. The subduction velocity V_s is then determined as the algebraic sum of trench and plate velocities: $V_s = V_p + V_t$. V_p is defined as positive when directed toward the trench, V_t is negative when directed toward the trench (Figure 1).

[23] Energy dissipation per unit of volume, Φ, by an incompressible fluid is measured as [*Ranalli*, 1995]:

$$\Phi = \eta \dot{\varepsilon}'_{ij} \dot{\varepsilon}'_{ij} \tag{8}$$

[24] We calculate Φ both over whole system and its fractions dissipated by the plate φ_l and the upper mantle φ_{um}. How the viscous dissipation is partitioned between plate and mantle is described as the percentage of the energy dissipated by the subducting lithosphere φ'_l:

$$\varphi'^{\%}_l = \frac{\varphi_l}{\Phi} = \frac{\varphi_l}{\varphi_l + \varphi_{um}} \tag{9}$$

[25] The energy dissipated by the plate and upper mantle are calculated for each numerical calculation time step. The fraction of energy used by lithosphere is a time averaged quantify over the "steady state phase" which is defined as the period after the interaction with the 660-km discontinuity, which is characterized by approximately constant velocities (see below).

3. Results

3.1. Reference Models

[26] All the calculations show the typical sequence of three phases during which plate and trench motions are distributed in different ways [*Funiciello et al.*, 2003b]: (phase I) the slab accelerates during the sinking within the mantle, (phase II) a transient interaction between slab and the 660-km discontinuity, and (phase III) a steady state condition, in which a constant velocity (for trench, plate, and subduction) and invariable slab geometry are achieved. As a general rule, the motion of slab during the steady state phase can be classified in (1) a retreating (or slab roll-back) mode for which $V_t > 0$, V_p is low, and the slab dip is shallow and (2) an advancing mode with $V_t < 0$, V_p is high, and the slab dip is steep (Figure 1). Sometimes, the slab shows a transitional behavior, starting its migration in advancing style, and later, after folding on the discontinuity, changing to retreating mode during the steady state phase. We refer to this case as the "fold-and-retreat" mode (see Animations 5 and 6 (Model 6), available as auxiliary material[1]).

[27] All varied model parameters for each model are reported in Table 1. The temporal evolution and the rheological properties of our reference retreating mode model (Table 2, experiment 1) are described in Figure 2 and in Animations 1 and 2. During the first stage (phase I, Figure 2a) the slab sinks through the upper mantle. Acceleration of the process occurs because of the increase of the slab pull with the slab length through time, which also results in an increase of the energy dissipation (Figure 2f). The bending zone, where the plate at the surface deforms to sink into the mantle as a subducting slab experiences high deformation, and the directly surrounding mantle deforms to adjust to the slab motion. The trench begins to arch slightly (plan view, Figure 2c, phase I) because the trench migration results in a relative mantle that curves the edges on the slab.

[28] In the transient phase (phase II, Figure 2a), a short slowdown of the subducting process occurs during the first slab-discontinuity interaction (Figure 2e). The energy dissipated by the lithosphere in this stage is almost constant (Figure 2f), whereas the dissipation of the whole system drops, because the slow mantle flow dissipates less energy.

[29] During the last phase (phase III) a steady state situation is reached: the trench keeps retreating, and both plate and trench velocity are almost constant (Figure 2e). A large portion of the system energy is dissipated by plate in the slab bending zones, at the top and bottom (Figure 2b, phase III).

[1] Auxiliary materials are available in the HTML. doi:10.1029/2007GC001776.

Table 1. Parameters Used in the Models and Notations

Quantity	Symbol	Value
Gravitational acceleration	g	10 [m/s^2]
Domain length	L	4620×10^3 [m]
Domain depth	H	660×10^3 [m]
Domain width	W	4620×10^3 [m]
Initial plate length	l	2310×10^3 [m]
Plate thickness	h	$(58-100) \times 10^3$ [m]
Plate width	w	$(600-2310) \times 10^3$ [m]
Density contrast between slab and mantle	$\Delta\rho$	75–100 [kg/m^3]
Reference upper mantle viscosity	η_{um}	$10^{20}-10^{22}$ [Pa·s]
Lithosphere viscosity	η_l	$(5-20) \times 10^{23}$ [Pa·s]
Subduction velocity	V_s	[m/s]
Plate velocity	V_p	[m/s]
Trench velocity	V_t	[m/s]
Yield stress	τ_{yield}	[Pa]
Coefficient of internal friction	μ_f	[-]
Frictional cohesive strength	C_f	[Pa]
Angle of internal friction	α	[°]
Dynamic pressure	P	[Pa]
Strain rate	$\dot{\varepsilon}$	[s^{-1}]
Second invariant of the strain rate	$\dot{\varepsilon}'_{ij}$	[s^{-1}]
Dynamic shear viscosity	η	[Pa·s]
Total dissipated energy	Φ	[W]
Energy dissipated by plate	φ_l	[W]
Energy dissipated by upper mantle	φ_{um}	[W]
Relative plate dissipation	$\varphi_l^{\%}$	[%]

However, additional energy dissipation occurs in the wedge and between the slab and the box bottom. By now, the arc shape (in plan view) is very pronounced (Figure 2c, phase III). The effective viscosity (Figure 2d) illustrates the effect of pseudoplasticity. In the bending zone, viscosity undergoes a significant reduction relative to the reference plate viscosity. The subducted part of the slab is not affected by weakening for depths larger than approximately the thickness of the plate.

[30] Figure 3 and Animations 3 and 4 show a plate moving in advancing style (Table 2, experiment 3). When the slab begins to sink into the mantle (Figure 3a, phase I), the trench again migrates backward (i.e., in retreating mode). The process is accelerated by the increasing length of the slab (Figure 3e). Also the energy dissipated by both the plate and the system increases (Figure 3f). The trench is only slightly curved (Figure 3c, phase I).

[31] During the second phase (Figure 3a, phase II) subduction slows down (Figure 3e), the slab tip interacts with the 660-km discontinuity, and the trench inverts its direction and starts to move in advancing mode. Plate dissipation undergoes a reduction (Figure 3f), being approximately equally divided between the top and the bottom bending zones. The steady state phase (Figure 3a, phase III) is characterized by a plate velocity that is significantly higher than the trench velocity (Figure 3e), and by fairly constant energy dissipation (Figure 3f). The trench has no arc-shape, but edges slightly bend backward following the direction of the mantle return flow (Figure 3c, phase III). At the bending zone the viscosity undergoes a reduction, respect to the reference plate viscosity (Figure 3d).

Table 2. Model Parameters That Are Varied for Different Experiments: Density Contrast, Width, Thickness, and Viscosity of Upper Mantle and Plate[a]

Exp.	$\Delta\rho$, kg/m^3	w, km	h, km	η_{um}, Pas	η_l, Pas	Mode
1[b]	100	1320	58	10^{21}	10^{24}	ret
2	100	1320	67	10^{21}	10^{24}	ret
3[c]	100	1320	72	10^{21}	10^{24}	adv
4	100	1320	86	10^{21}	10^{24}	adv
5	100	1320	100	10^{21}	10^{24}	adv
6[d]	100	660	72	10^{21}	10^{24}	ret
7	100	924	72	10^{21}	10^{24}	adv
8	100	2300	72	10^{21}	10^{24}	ret
9	125	1320	58	10^{21}	10^{24}	ret
10	125	1320	72	10^{21}	10^{24}	ret
11	125	1320	86	10^{21}	10^{24}	adv
12	150	1320	58	10^{21}	10^{24}	ret
13	150	1320	72	10^{21}	10^{24}	ret
14	150	1320	86	10^{21}	10^{24}	ret
15	150	1320	100	10^{21}	10^{24}	adv
16	100	1320	72	10^{22}	10^{25}	adv
17	100	1320	72	10^{20}	10^{23}	adv
18	100	1320	72	10^{21}	5×10^{23}	ret
19	100	1320	72	10^{21}	2×10^{24}	adv
20	100	1320	72	10^{20}	10^{24}	adv
21	100	1320	72	10^{22}	10^{24}	ret
22–26	75	-	58–114	10^{21}	10^{24}	ret-adv
27–31	100	-	58–114	10^{21}	10^{24}	ret-adv
32–36	125	-	58–114	10^{21}	10^{24}	ret-adv
37–41	150	-	58–114	10^{21}	10^{24}	ret-adv
38–41	75	-	58–114	10^{21}	5×10^{23}	ret-adv
47–51	100	-	58–114	10^{21}	5×10^{23}	ret-adv
52–56	125	-	58–114	10^{21}	5×10^{23}	ret-adv
57–61	150	-	58–114	10^{21}	5×10^{23}	ret
62–66	75	-	58–114	10^{21}	2×10^{24}	ret-adv
67–71	100	-	58–114	10^{21}	2×10^{24}	ret-adv
72–76	125	-	58–114	10^{21}	2×10^{24}	ret-adv
77–81	150	-	58–114	10^{21}	2×10^{24}	ret-adv

[a] Models 1, 3, and 6 are available in the auxiliary material.
[b] Model 1: reference experiment of the retreating style.
[c] Model 3: reference experiment of the advancing style.
[d] Model 6: fold-and-retreat subduction style case.

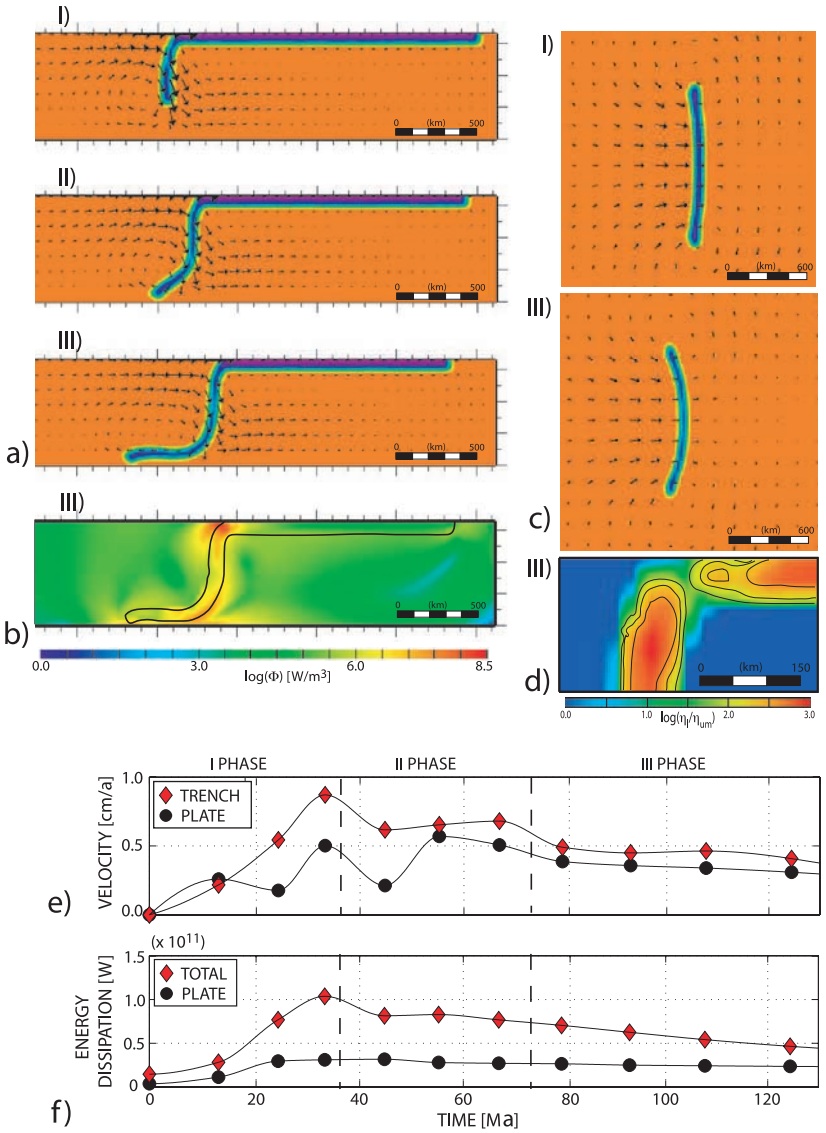

Figure 2. Description of retreating slab. (a) Lateral views of compositional field, (b) visualization of the energy dissipated by plate and upper mantle, (c) top view of the compositional field, (d) viscosity field at the bending zone, (e) the evolution of the trench and plate velocities, and (f) the energy dissipation for the system and the plate versus time. The roman numerals I, II, and III indicate if the snapshot is taken in the first, second, or third phase of the subducting process at 24.9, 45.5, and 79.8 Ma after model start. Vertical cross sections are taken through the middle of the plate (y = 2310 km). Horizontal cross sections are taken at 200 km depth from the top. Black arrows illustrate the vertical and horizontal flow pattern in the mantle. Black line in the energy visualization represents the slab contour. In Figure 2e, red diamonds represent trench velocity, and black dots represent plate velocity. In Figure 2f, red diamonds represent the energy dissipated by the whole slab/mantle system, and black dots represent the energy dissipated by the lithosphere. Full time evolution (top and lateral view) can be seen in the Model 1 animations (Animations 1 and 2).

3.2. Role of Plate Thickness, Viscosity, and Density

[32] Sensitivity analysis provides a basic understanding of the system by systematic variation of the parameters. Two-dimensional and three-dimensional models are performed by systematically changing each of the geometrical (h, w) and rheological ($\Delta\rho$, η_l/η_{um}) parameters over a wide range (Table 2).

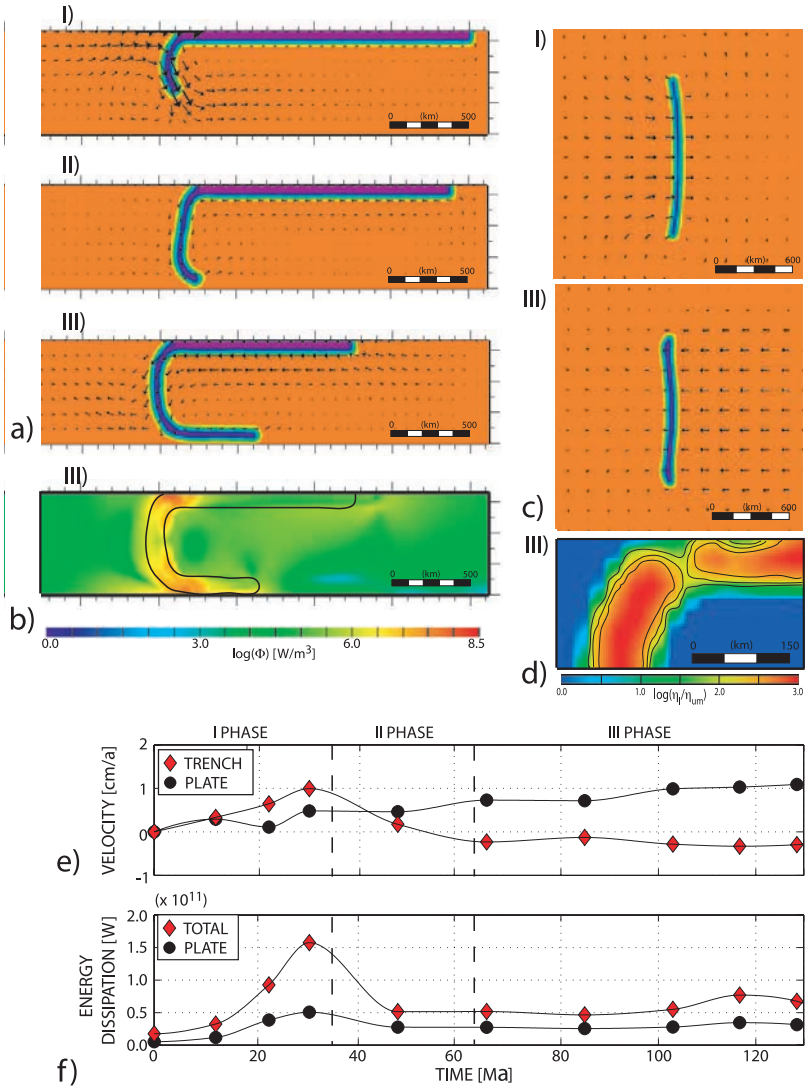

Figure 3. The same as Figure 2, but for an advancing slab (model run 3). The snapshot is taken in the first, second, or third phase of the subducting process at 22.9, 48.6, and 116.7 Ma after model start. A full time evolution (top and lateral view) can be seen in the Model 3 animations (Animations 3 and 4).

3.2.1. Effects of the Pseudoplasticity on the Plate Strength

[33] Before showing the results about the influence of the investigated parameters on the trench migration it is useful to discuss the role of the pseudoplasticity in the lithosphere strength. The coefficient of friction μ_f of most rocks is between 0.6 and 0.8 under dry conditions [*Turcotte and Schubert*, 1982; *Kohlstedt et al.*, 1995]. The presence of water throughout the Earth's crust affects the friction and therefore lowers the stress at which the fracture occurs. This results in a lower effective friction coefficient.

[34] This friction coefficient significantly influences the subduction style and vigor, and we first derive an "optimal" value for μ_f, for which we obtain a realistic slab shape and no slab necking. These calculations have been performed in the 3-D domain that more realistically simulates the Earth. The rheological and geometrical features of the plate are the same for all calculations: h = 72 km, w = 1320 km, $\Delta\rho$ = 100 kg/m^3, $\eta_l/\eta_{lum} = 10^3$. For μ_f = 1.0, a dripping instability occurs, since the uppermost lithosphere is very stiff and resists detaching from the surface. For $\mu_f \leq 0.01$, on the other hand, the slab is drastically weakened, which results in a non-coherent slab. Intermediate values of μ_f around 0.1 show a qualitatively reasonable subduction zone and those values are further compared to subduction velocities in laboratory modeling results of *Bellahsen et al.* [2005], in which a

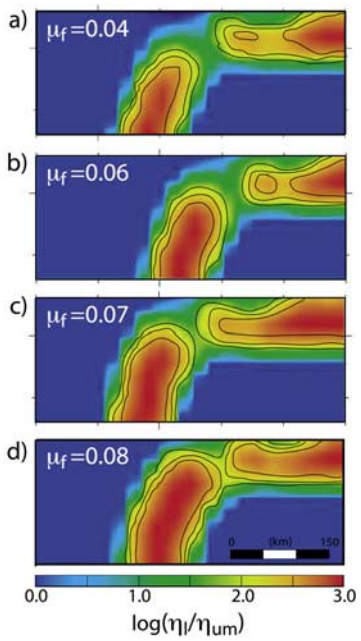

Figure 4. Descriptions of the viscosity field for different values of the friction coefficient: μ_f = (a) 0.04, (b) 0.06, (c) 0.07, and (d) 0.08.

very comparable model setup to ours is used, although without pseudoplastic yielding. Afterward, a similar approach has previously been used by *Schott and Schmeling* [1998] and *Enns et al.* [2005] by adjusting μ_f to obtain subduction velocities that reasonably compare to natural values. The viscosity field is largely affected by the pseudoplasticity (Figure 4). A friction coefficient μ_f = 0.04/0.06 drastically lowers the lithospheric viscosity at the bending zone (Figures 4a and 4b), whereas the low viscosity region becomes smaller for μ_f = 0.07 (Figure 4c). With μ_f = 0.08 such low viscosity at the bending zone is reduced to more shallow areas (Figure 4d). As well as affecting the strength of the lithosphere, the weakening influences the style of subduction and its kinematics. The plate with μ_f = 0.04 and 0.06 migrates in retreating style (Figure 5). The plate with μ_f = 0.07 folds on the bottom of the box and that with μ_f = 0.08 moves in advancing style.

[35] The percentage of the energy dissipated by the lithosphere in the steady state phase increases with the coefficient (from ~27% to 52% of the total energy; Figure 5).

[36] Through the comparison with the laboratory model velocities, our preferred value for μ_f is 0.08. This frictional coefficient is an order of magnitude lower than that found by laboratory experiments performed on real rocks, but it is consistent with the modeling results obtained by *Schott and Schmeling* [1998] (μ_f = 0.07) and *Enns et al.* [2005] (μ_f = 0.1). Furthermore, *Moresi and Solomatov* [1998] found that, in a mantle convection model with temperature-dependent viscosity, a mobile-lid regime develops in the Earth if μ_f is less than approximately 0.03-0.13. Such range also corresponds to values obtained from seismic field studies [*Kanamori*, 1994].

3.2.2. Two-Dimensional Models

[37] Two-dimensional models can be regarded as three-dimensional models with no variation in the third dimension (i.e., the y direction in our setup). Such setup is a reasonable approximation for of the many wide subduction zones on Earth. Since 2-D models are less computationally demanding than their 3-D equivalents, 2-D models are ideally suitable for large parameter sensitivity studies.

[38] In the following models we vary the plate thickness h from 58 to 114 km for different density contrasts $\Delta\rho$ (75–150 kg/m^3) and different viscosity ratio η_l/η_{um} (500–2000), using upper mantle viscosity η_{um} of 10^{21} Pa·s. This gives a total of 60 calculations (Figure 6). In Figure 6, the velocity ratio V_p/V_s is used to illustrate the subduction style:

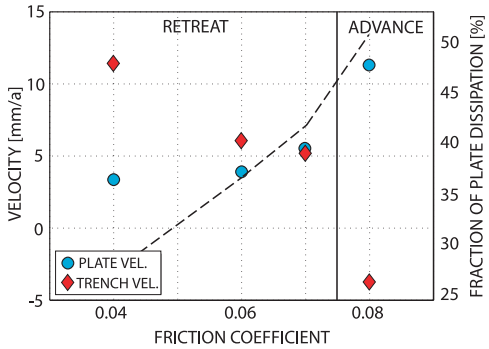

Figure 5. Plot of the plate and trench velocity and the fraction of energy dissipated by the lithosphere in function of the coefficient of friction. Light blue dots represent the plate velocity; red diamonds represent the trench velocity. The black dashed line represents the fraction of the plate dissipation. The solid line determines the transition between the retreating style and the advancing style.

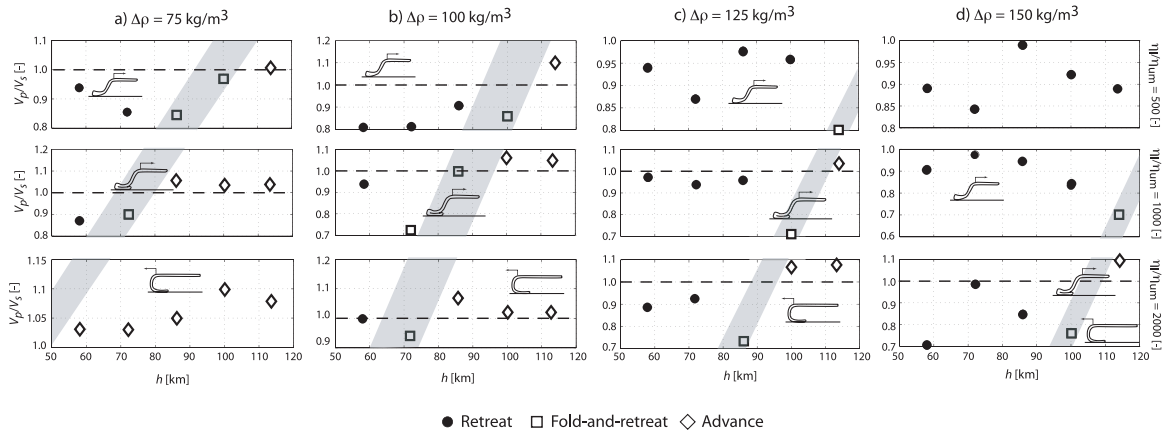

Figure 6. Ratio between plate velocity and subduction velocity V_p/V_s versus plate thickness h for different viscosity ratio and density contrast, in 2-D models. (a) Velocity ratio for $\Delta\rho = 75$ kg/m^3, (b) velocity ratio for $\Delta\rho = 100$ kg/m^3, (c) velocity ratio for $\Delta\rho = 125$ kg/m^3, and (d) velocity ratio for $\Delta\rho = 150$ kg/m^3. Dots, squares, and diamonds represent retreating, fold-and-retreat, and advancing styles, respectively. The dashed line is $V_p/V_s = 1$. The grey region represents the transition zone between retreating style and advancing style in the model calculations.

$V_p/V_s > 1$ corresponds to advancing mode subduction, while $V_p/V_s < 1$ shows retreating mode or fold-and-retreat slabs.

[39] Generally, the thinner plates subduct within the mantle with trench retreating, the thicker ones overturn in the advancing mode. The intermediate slabs show the fold-and-retreat mode. This trend is visible for high η_l/η_{um} (1000–2000) and less dense slabs (75, 100, 125 kg/m^3). In general, the fraction of the energy dissipation in the lithosphere increases with increasing thickness of the plate (Figure 7). The maximum of the energy is dissipated by the folding plates. Advancing slabs dissipate less energy than the folding case but more than the retreating slab with the same density.

[40] Next, we illustrate the effects of the density contrast $\Delta\rho$ using the same set of model calculations. Figure 6 illustrates that an increase of the density contrast favors the retreating style. For $\Delta\rho =$ 150 kg/m^3, the advancing style is not obtained for reasonable plate thickness and the viscosity ratio. From an energetic point of view, for models with $\eta_l/\eta_{um} = 500$, a higher density contrast leads to a lower fraction of energy dissipated by the lithosphere (Figure 7). The energy to deform the plate is on average 50% of the total energy for $\Delta\rho =$ 75 kg/m^3 and, and around 30% for $\Delta\rho = 150$ kg/m^3. For $\eta_l/\eta_{um} = 1000$ and 2000, the energy dissipated by slabs moving with the same subduction style is almost constant: 35% for the retreating mode and 40% for the advancing one.

[41] Next we examine the effects of the viscosity ratio η_l/η_{um} (Figure 6). We find that the increase of η_l/η_{um} favors the advancing style: the transition from retreating to advancing mode shifts toward thinner plates for higher η_l/η_{um}. For higher viscosity contrasts, less energy is dissipated by the slab and more by the mantle, for both subduction styles (Figure 7).

3.2.3. Three-Dimensional Models

[42] The same approach used for the 2-D model results is followed for the 3-D models, but a smaller number of calculations are performed because of their computational demand (Table 2).

[43] Qualitatively, similar results are obtained for these 3-D models. By increasing the plate thickness, the advancing style of subduction is favored, as is the case for a lower density difference between the lithosphere and the upper mantle, and a higher viscosity ratio (Figures 8 and 9).

[44] Nevertheless, there are a few interesting differences between 2-D and 3-D model results. The range of V_p/V_s is much larger for 3-D models than it is in 2-D. The V_p/V_s ratio is around 0.5 for the retreating case, and around 1.5 for the advancing case, whereas in 2-D models, V_p/V_s values are distributed very close to the threshold $V_p/V_s = 1$. In addition, in 3-D geometry obviously another degree of freedom enters the subduction parameter space: the width of the plate.

3.2.4. Effects of Plate Width

[45] Here, we vary the width of the plate w between 600 and 2300 km, while h is kept constant at 72 km,

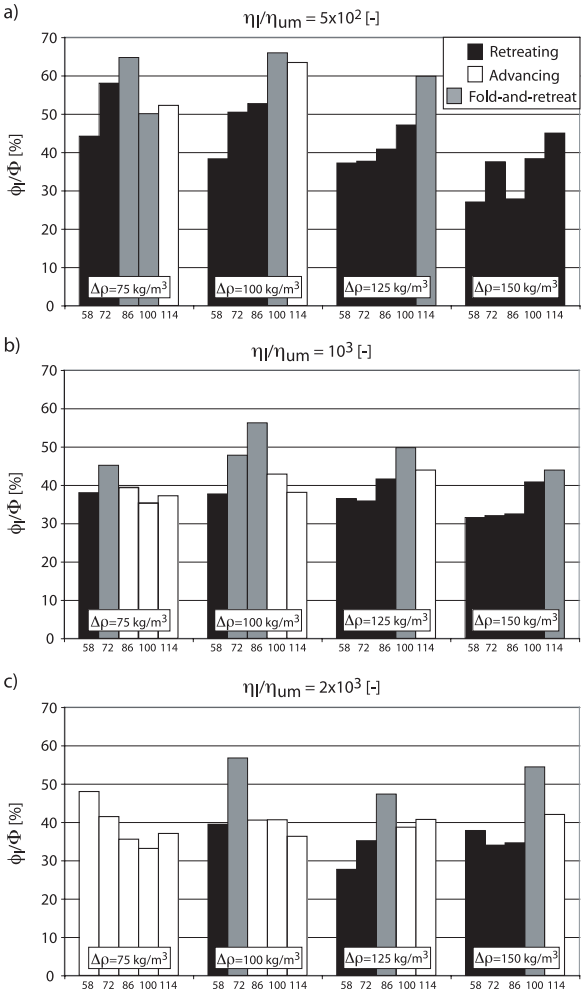

Figure 7. Percentage of the energy dissipated by 2-D slabs in function of the viscosity ratio: (a) $\eta_l/\eta_{um} = 5 \times 10^2$, (b) $\eta_l/\eta_{um} = 10^3$, and (c) $\eta_l/\eta_{um} = 2 \times 10^3$. The energy fraction is measured for each density contrast and plate thickness. The style of subduction is marked by different bar colors.

$\Delta\rho$ at 100 kg/m^3 and η_l/η_{um} at 10^3 (Figure 10). We find that the largest plate (w = 2300 km) favors the retreating style, the intermediate plates (w = 924/1320 km) move in advancing style and the narrowest one (w = 660 km) in fold-and-retreat mode. The retreating plate dissipates a fraction of ~46% of the total energy, the advancing ones 51% and the narrow fold-and-retreat one 55%.

3.3. Energy Dissipation

[46] We investigated how the energy dissipated in our subduction system is used and partitioned between the mantle and the downgoing lithosphere. We found that, in both 2-D (Figure 7) and 3-D models (Figures 8 and 9), most of energy dissipation occurs in the upper mantle, which accommodate the slab motion. The dissipation is between 50% and 70% of Φ for 2-D models, and around 55% for 3-D models and is concentrated at the wedge and at the region between the slab and the 660-km discontinuity, where the overpressure is large.

[47] Energy dissipation in the plate is concentrated at the bending zones, near the surface and at depth. On average, strong (advancing) slabs dissipate more than the weak (retreating) slabs, for which the unbending occurs easily, but less than folding slabs (~55%). The folding mechanism requires a large amount of energy to deform the slab several times.

[48] The plate contribution to the total dissipation decreases by increasing the viscosity ratio reflecting the increase of the plate stiffness, and the consequent reduction of the plate deformation.

4. Discussion

[49] The subduction style can be classified using the motion of the trench that can be either retreating or advancing with respect to the upper plate [*Faccenna et al.*, 2007]. Retreating trench style is usually more frequent [*Garfunkel et al.*, 1986]. However, the exact estimation of the amount of retreating or advancing trench over the Earth surface depends upon the chosen reference frame. For example, *Heuret and Lallemand* [2005] estimate that 53% of the total trench length is advancing in the HS3 reference frame [*Gripp and Gordon*, 2002]. This percentage decreases to 30% and to 39% taking the GJ86 [*Gordon and Jurdy*, 1986] or NNR [*DeMets et al.*, 1994] reference frame, respectively. In our models we obtain both subduction modes with a realistic range of geometrical and rheological parameter settings.

4.1. Reducing the Complexity of the Subduction System

[50] The 60 2-D model calculations, in which $\Delta\rho$, h, and η_l/η_{um} are varied (Table 2), are used to determine the relationship between model parameters and subduction style (Figures 11 and 12). A pattern can be recognized: dense (high $\Delta\rho$), thin (low h), and relatively low viscous (low η_l/η_{um}) slabs tend to subduct in retreating mode, while less dense, thicker or more viscous slabs have a tendency to go into the advancing mode. We fitted the modeling results to a unifying parameter S of the

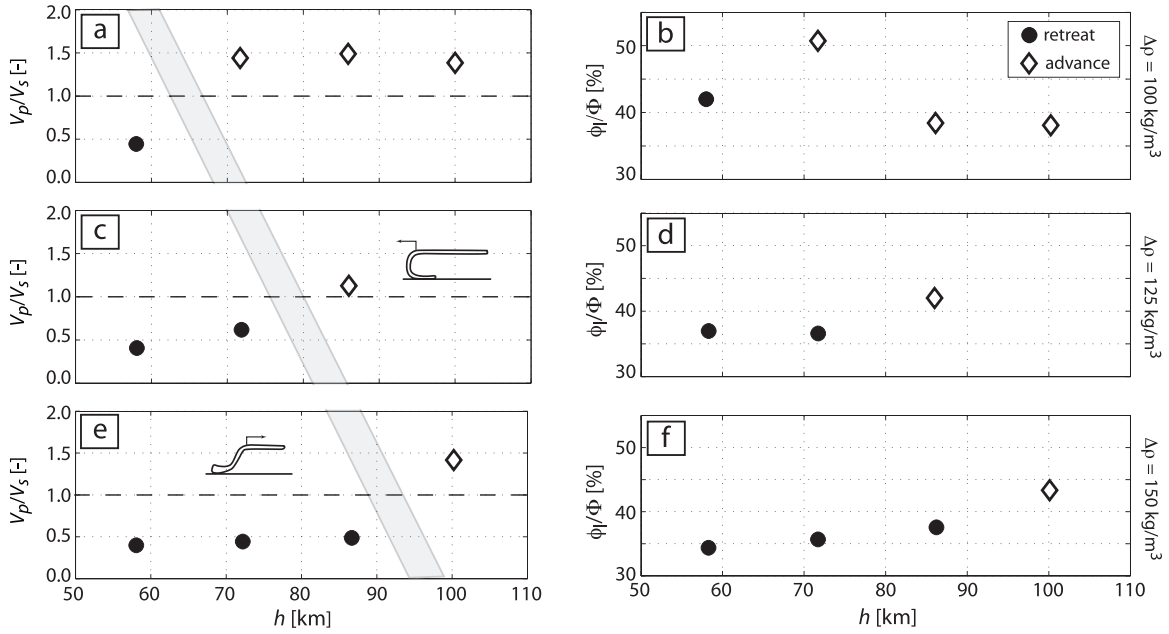

Figure 8. Ratio between plate velocity and subduction velocity versus plate thickness by varying the density contrast, in 3-D models. The viscosity ratio η_l/η_{um} and the plate width are kept fixed at 10^3 and 1320 km, respectively. (a) Velocity ratio for $\Delta\rho$ = 100 kg/m^3, (b) fraction of the energy dissipated by lithosphere for $\Delta\rho$ = 100 kg/m^3, (c) velocity ratio for $\Delta\rho$ = 125 kg/m^3, (d) fraction of the energy dissipated by lithosphere for $\Delta\rho$ = 125 kg/m^3, (e) velocity ratio for $\Delta\rho$ = 150 kg/m^3, and (f) fraction of the energy dissipated by lithosphere for $\Delta\rho$ = 150 kg/m^3. Dots represent retreating slabs, and diamonds represent advancing ones. The dashed line is V_p/V_s = 1. The grey region represents the transition zone between retreating style and advancing style.

subducting plate with the following linear scaling law:

$$S = A \ln\left(\frac{\eta_l}{\eta_{um}}\right) + Bh + C\Delta\rho \qquad (10)$$

[51] We will refer to S as the stiffness parameter for reasons explained below. We fit the scaling law parameters A, B, and C such that S = 1 describes as closely as possible the transition between retreating and advancing mode subduction. Best fitting parameters are A = 0.1233 [−], B = 0.0049 [m^{-1}] and C = −0.0032 [m^{3}kg^{-1}], and the results for S = 1 are indicated by the solid lines in Figures 11 and 12. Except for a few outliers, the scaling law

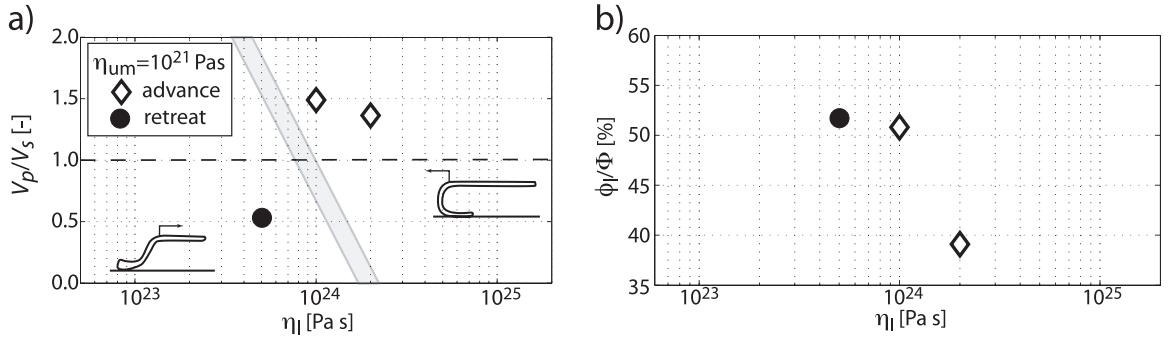

Figure 9. (a) Ratio between plate velocity and subduction velocity for 3-D cases with different lithosphere viscosity and fixed upper viscosity η_{um} = 10^{21} Pas. The density contrast $\Delta\rho$ between lithosphere and upper mantle and the plate width are kept constant at 10^3 and 1320 km, respectively. (b) The corresponding energy dissipated by the lithosphere. Dots represent retreating slabs, and diamonds represent advancing ones. The dashed line is V_p/V_s = 1. The grey region represents the transition zone.

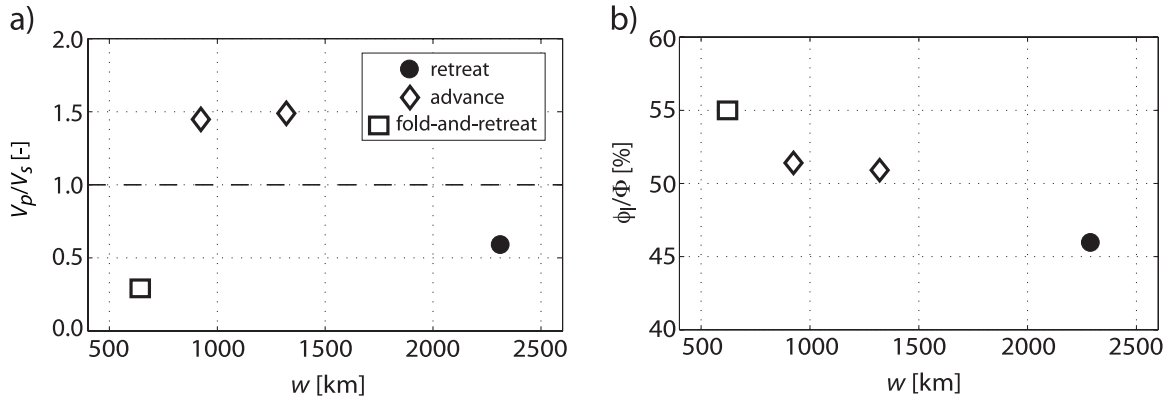

Figure 10. (a) Ratio between plate velocity and subduction velocity versus plate width for 3-D case. (b) The percentage of energy dissipated by lithosphere versus plate width. The density contrast $\Delta\rho$ and the viscosity ratio η_l/η_{um} are kept constant at 10^2 and 10^3, respectively. Dots represent retreating slabs, the diamonds represent advancing slabs, and squares represent the folding ones. The dashed line is $V_p/V_s = 1$.

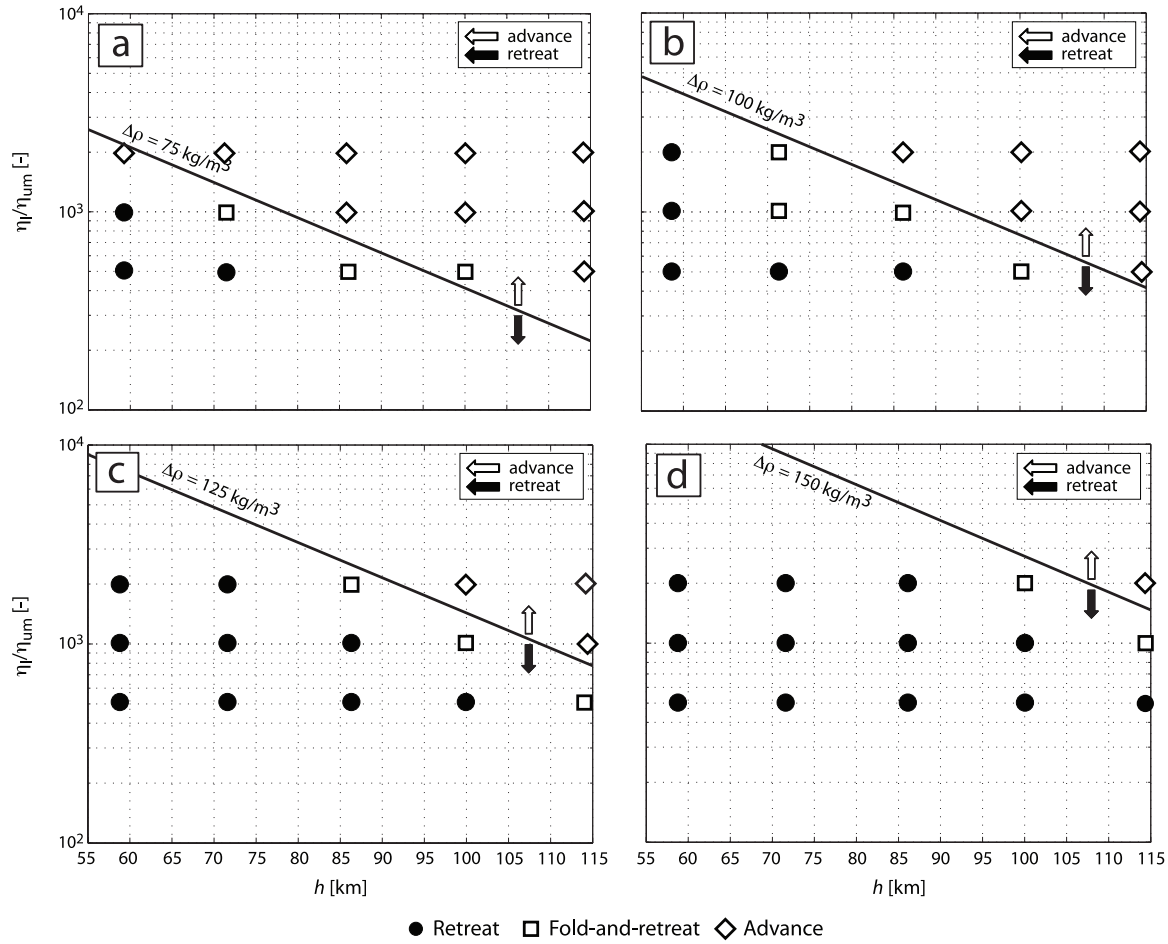

Figure 11. Comparison between our results and the scaling law for fixed density contrast: (a) $\Delta\rho$ = 75 kg/m^3, (b) $\Delta\rho$ = 100 kg/m^3, (c) $\Delta\rho$ = 125 kg/m^3, and (d) $\Delta\rho$ = 150 kg/m^3. The arrow indicates the direction toward which the retreating or the advancing style occurs, with respect to the solid line representing a fixed trench, $V_p/V_s = 1$. Dots represent retreating slabs, diamonds represent advancing slabs, and squares represent the folding ones.

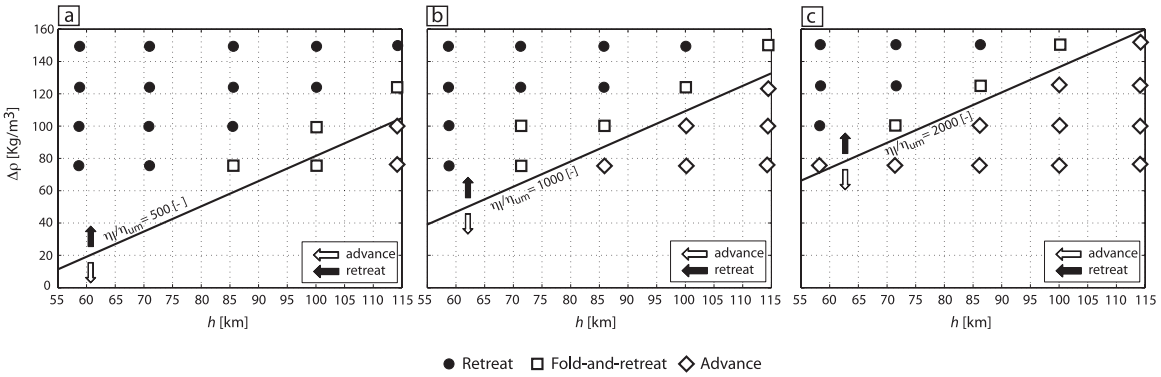

Figure 12. Comparison between the numerical results and the scaling law for fixed viscosity ratio: (a) $\eta_l/\eta_{um} = 5 \times 10^3$, (b) $\eta_l/\eta_{um} = 10^3$, and (c) $\eta_l/\eta_{um} = 2 \times 10^3$. The arrow indicates the direction toward which the retreating or the advancing style occurs, with respect to the solid line representing a fixed trench, $V_p/V_s = 1$. Dots represent retreating slabs, diamonds represent advancing slabs, and squares represent the fold-and-retreat cases.

(equation (10)) with $S = 1$ describes well the transition between advancing and retreating subduction (Figures 11 and 12). Now $S < 1$ and $S > 1$ correspond to subduction in retreating and advancing style, respectively. S can be interpreted as an effective stiffness of the subducting plate: increasing η_l/η_{um} (resulting in a more viscous plate) or h (a thicker plate) obviously increases its "stiffness" S, which is reflected by the positive values for A and B. The negative relation between $\Delta\rho$ and S ($C < 0$) is less obvious and requires some explanation: an increased plate density increases the gravitational instability, and therefore the stresses that drive the subduction. This, in turn, results in more yielding due to the pseudoplasticity, and a reduction of the effective viscosity in these yielding areas. So increasing $\Delta\rho$ reduces locally the stiffness of the plate.

[52] The stiffness of the plate appears to be the most important ingredient in controlling the subduction behavior. A similar conclusion was experimentally drawn by *Ribe* [2003] for a sheet of viscous fluid being dropped onto a surface.

[53] Strong slabs ($S > 1$) preserve their bended shape during the subduction process with little possibility to unbend. Hence slabs reach the 660-km discontinuity with a backward-reclined shape (Figure 3a, phase II). Weak slabs ($S < 1$), on the contrary, are easily deformed after subduction, and descend sub-vertically within the upper mantle (Figure 2). They are able to unbend before reaching the 660-km discontinuity. The fold-and-retreat cases are somewhat more complicated. As with the "strong" slabs, the tip reaches the 660-km discontinuity such that an advancing motion is favored. But advancing mode subduction requires more rapid surface plat motion than retreating mode subduction (Figures 2e and 3). If a plate cannot keep up with this required surface motion, it folds up on the discontinuity and continues in the retreating mode. In our models the bending/unbending has no elastic component. However, *Capitanio et al.* [2007] showed that, by varying the Young's modulus and the Poisson's ratio, the large-scale motion and stresses are not influenced by the presence of the elasticity.

[54] In order to investigate how the initial plate shape influences the mode of subduction, we performed two calculations in which we change halfway the plate thickness, such that thin plate subduction is followed by thick-plate subduction or vice versa. The change from thin to thick plate subduction (or vice versa) causes a change from retreating to advancing subduction (or vice versa). This illustrates that the subduction modes does not depend on the initial plate configuration, but on the plate strength.

4.2. Role of the Viscosity

[55] Dimensionalized velocities in our numerical models are all fairly low. But it is worthwhile pointing out that those velocities scale directly with $1/\eta$. The used viscosity scale does not affect the style of subduction at all, but only affects the timescale of the subduction process. We confirmed this by performing a few calculations by keeping η_l/η_{um} constant at 10^3 and by varying η_{um}. By decreasing η_l and η_{um} by a factor of 10, all velocities increase by the same factor, but otherwise results are identical. Therefore, if all our results are translated in terms of 10^{20} Pas upper mantle viscosity, trench velocity will range be-

tween −6 and 15 cm/a. These values are in very good agreement with trench velocities of subduction zones on Earth that go from −6 up 13 cm/a [*Heuret and Lallemand*, 2005]. Thus we argue that $\eta_{um} = 10^{20}$ Pas is the best fitting value to compare the numerical models to the natural cases.

[56] *Stegman et al.* [2006] performed calculations with a very similar numerical model setup. However, they obtained only retreating trench migration and no advancing slabs. This is probably because the viscosity ratio imposed between the lithosphere and the upper mantle is much lower (100–200) than in our case. Such low viscosity ratio leads to a small stiffness *S*, and therefore favors retreating style subduction. Although *Stegman et al.* [2006] use a reference $\eta_{um} = 10^{20}$ Pas, the largest observed retreat rate is only 4 cm/a and a plate velocity of 0.5 cm/a. The most likely reason of these low velocities can again be the related to the low viscosity ratio imposed between the lithosphere and the upper mantle. This acts to weaken the slab and reduces the possibility to become an efficient stress guide to pull the surface plate into the subduction zone.

[57] Despite the setup of the numerical models by *Billen and Hirth* [2007] being significantly different from our one, they also found that the slab strength and a higher viscosity contrast between plate and mantle controls primarily the evolution and the dip of the slab during its sinking.

[58] Funiciello et al. (submitted manuscript, 2007) show experimentally that, in order to obtain the variability of the subduction styles recognized in nature, it is necessary that the lithosphere/upper mantle viscosity ratio ranges between 150–500. This interval is somewhat lower than that found out in our numerical model range from 500 to 2000. This discrepancy can be understood by taking into account that the presence of the pseudoplasticity at the uppermost part of the lithosphere in the numerical models effectively reduces the viscosity of the slab in the bending zone (by approximately a factor 130 for weak slabs and ∼450 for stronger slabs) in our numerical calculations, while such viscosity reduction is absent in the laboratory models.

4.3. Role of the Pseudoplasticity at the Bending Zone

[59] In our models, the pseudoplastic deformation enables a subducting plate to decouple from the free-slip, but vertically fixed surface. On Earth, the surface moves freely up and down, and such weakening may not be strictly necessary for subduction to occur. Nonetheless, a similar mechanism can be expected occur on the Earth from lithospheric breaking and weakening before its entrance at trench [*Ranero et al.*, 2005; *Billi et al.*, 2006; *Hirano et al.*, 2006]. Subducting plates suffer significant crustal-scale faulting as revealed by observations of seafloor bathymetry and seismic reflections data at several subduction zones [*Kobayashi et al.*, 1998; *Ranero et al.*, 2003]. In fact, the negative buoyancy of the slab itself creates the stresses to deform and weaken the plate at the bending zone [*Billen and Gurnis*, 2001]. Moreover, the presence of the oceanic sediment at the trench or wet rock conditions results in a low friction coefficient. Our results suggest that strong plates favor an advancing trench motion, while weaker plates result in trench retreat. This is similar to what is observed on Earth [*Heuret and Lallemand*, 2005; *Faccenna et al.*, 2007], where older, stronger plates give more trench advance due to the absence of pseudoplasticity in those models. Therefore, we hypothesize that on Earth, pseudoplasticity plays an important role in subduction dynamics, similar to our numerical experiments.

4.4. Role of the Plate Width

[60] The width of the plate affects the style of subduction as well. Plates with large width ($w >$ 2300 km) tend to have a retreating mode, intermediate plates (900 km $< w <$ 2300 km) an advancing trend. This result is in agreement with *Bellahsen et al*. [2005], who investigate with analogue models the effect of plate width on trench migration.

[61] Because our models, in which we vary *w*, have the same h, $\Delta\rho$ and η_l/η_{um}, the plates have the same stiffness *S*. Therefore, as discussed above the change of subduction style cannot be due to a change in plate stiffness, and should be explained in terms of mantle flow and plate/mantle shear drag force.

[62] The style of subduction is determined by how the tip of the slab reaches the 660-km discontinuity. Intermediate and wide plates show exactly the same shape and dip during the first phase of the process, because they have the same strength. When the slab tip is approaching the bottom of the box, the mantle overpressure created by the wide plate is larger than that created by the intermediate one. The mantle opposes the slab sinking and a vigorous upward flow occurs. This mechanism leads the tip a bit forward, allowing the consequent retreating mode subduction.

[63] In general, wide plates stir a larger amount of mantle material than the intermediate ones [*Piromallo et al.*, 2006, *Funiciello et al.*, 2006]. This causes a more vigorous horizontal flow that is reflected into a high fraction of the dissipated energy. At the same time, a high shear drag acts at the base of the plate opposing the plate motion.

[64] The narrow plate initially moves in advancing style. The involved slab pull force is less than that of the intermediate plate and the subduction process is slower, but at the same time the shear drag is higher than the intermediate cases, because the shear at the non-negligible surface area of the plate sides starts to play a role. At the certain point, the slab is not able to pull down further lithospheric material and the trench migrates in retreat.

[65] The scaling law may be applied to the 3-D results with some adjustment, because at the moment, it is tuned for very wide plates: the 2-D model has, by definition, a laterally totally constrained configuration, which can be compared to an infinite trench extent.

[66] Our results appear in contrast with *Schellart et al.* [2007], who used numerical simulations to test the dependence of trench motion on slab width observed by *Bellahsen et al.* [2005]. As previously found by *Stegman et al.* [2006], *Schellart et al.* [2007] show that their trench retreat inversely scales with its width: wide plates are nearly stationary, intermediate ones prefer move in retreat and fold. In particular, this relationship becomes pronounced during the very late stage evolution of a narrow slab, when model evolution results can be strongly influenced by the unlikely limited length of the remaining subducting plate. The folding of the wide and intermediate slabs on the 660-km discontinuity is favored by the weakness of the plate. The low viscosity ratio of 200 between lithosphere and upper mantle and the viscoplasticity applied in the whole upper half of the plate [*Schellart et al.*, 2007, Supplementary Information] make the slab a non-efficient stress guide. In addition, the presence of a higher viscous lower mantle favors the piling of the lithosphere material. Besides, results from both Stegman et al. and Schellart et al. results are out of scale for V_p, which are approximately one order of magnitude lower than the observed plate velocities. Hence the trench migration V_t for the slabs may be overestimated (T. W. Becker and C. Faccenna, A review of the role of subduction dynamics for regional and global plate motions, submitted to *International Journal of Earth Sciences*, 2007).

4.5. Differences Between 2-D and 3-D Models

[67] From Figure 6 and Figure 9 it is clear that for the 2-D models the ratio between the plate and subduction velocity is very close to 1, a little bit lower than 1 (0.85–0.95) for the retreating slabs, a little bit higher than 1 (∼1.1) for the advancing slabs. A ratio equal to 1 means that the trench velocity is zero. In 3-D models the ratio results around 0.6 for the retreating trenches and around 1.5 for the advancing ones. This larger variation for 3-D results is due to the three-dimensionality of the system that allows the upper mantle to flow laterally around the slabs to facilitate trench migration. In 3-D the subduction style is maintained more easily than the 2-D case, and the fold-and-retreat case occurs less frequently.

4.6. Energy Balance

[68] In our models energy dissipation occurs mainly in the upper mantle, which accommodates the slab motion. Lithosphere dissipation is between 30% and 50% of the total Φ for 2-D models, and around 45% for 3-D models. These results are in agreement with those obtained by *Capitanio et al.* [2007]. *Conrad and Hager* [1999] analytically and numerically calculated the energy balance of a subduction system. They found that a thicker and/or more viscous slab dissipate more energy to deform and bend than a thinner and less viscous plate. In spite of this resembling result, a direct comparison is not possible because in their models the slab is constrained by a fixed trench position and radius of curvature, while in our dynamic models the plate is free to move. Few differences occur in the analogue experiments. In the work of *Bellahsen et al.* [2005], the bending force appears as the most important resisting contribution, ranging between 69% and 99% of the total energy. On the contrary, *Schellart* [2004] found that the bending resistance consumes around 30% of the total energy. But obviously, experimental energy dissipation estimates inevitably suffer from low accuracy in determining the roles of (bending) forces in analogue models.

5. Conclusions

[69] In this study, we have investigated 2-D and 3-D numerical models to analyze the dynamics of the subduction process. Our results show a significant and complex dependence of the mode of subduction (a retreating or advancing trench) on

several geometrical and rheological parameters. Advancing style subduction is promoted by a large plate thickness, a large viscosity contrast between plate and mantle, or a small density contrast between plate and mantle. Thin plates, with relatively low viscosity, or relatively high density, on the other hand, promote subduction in the retreating style (i.e., with slab roll-back). Realistic subduction occurs only for a pseudoplastic friction coefficient around 0.1 or somewhat less. Within this narrow range, lower values of this friction coefficient favor retreating subduction style. Therefore, a variation of the pseudoplasticity in the plate may have the same influence of a change of the model parameters. The width of the subducting plate shows a complicated relationship with the subduction style: both very narrow and very wide plates show retreating style subduction, while intermediate-width plates subduct in advancing mode. The change of the subduction style is not due to a variation in plate stiffness, but in terms of mantle flow and plate/mantle shear drag force. The complexity of this multiparameter system can be reduced significantly by recognizing that most of those model parameters have a clear relationship with the strength (or stiffness) of the plate. To that end, we developed a scaling law: $S = 0.1233 \ln(\eta_l/\eta_{um}) + 0.0049\ h - 0.0032\ \Delta\rho$, where S is a measure for the stiffness of the plate. For $S < 1$ (weak plates), retreating style subduction occurs, while for $S > 1$ (strong plates), subduction occurs in advancing style.

[70] Advancing slabs spent a larger percentage of the energy dissipation (55%) than retreating ones (45%). In particular, most of viscous energy dissipation occurs in the mantle to accommodate the slab motion, whereas the dissipation of the lithosphere (~30–50%) is mainly concentrated at the bending zones, both at the trench and at depth.

[71] Our results indicate that in order to have both advancing and retreating styles of subduction occurring, the viscosity ratio between plate and mantle needs to be within the range of 500–2000, although weakening by pseudoplastic yielding reduces this value significantly in the vicinity of the subduction zone. Furthermore, our model shows the observed range of plate velocities (from −6 to 13 cm/a) [*Heuret and Lallemand*, 2005] for a mantle viscosity of 10^{20} Pa s.

Acknowledgments

[72] We thank Susanne Buiter and Scott King for their careful reviews as well as the Editor Peter van Keken, who improved the early version of the manuscript. E.D.G. would like to thank Paul Tackley for providing the computational resources and Thorsten W. Becker, Lapo Boschi, Saskia Goes, Gabriele Morra, and Neil Ribe for discussions. The research by E.D.G. and F.F., as part of the Eurohorcs/ESF–European Young Investigators Awards Scheme, was partly supported by funds from the National Research Council of Italy and other National Funding Agencies participating in the 3rd Memorandum of Understanding, as well as from the EC Sixth Framework Programme. Publication 1518 of the Institute of Geophysics, ETH, Zürich.

References

Bellahsen, N., C. Faccenna, and F. Funiciello (2005), Dynamics of subduction and plate motion in laboratory experiments: Insights into the "plate tectonics" behavior of the Earth, *J. Geophys. Res.*, *110*, B01401, doi:10.1029/2004JB002999.

Billen, M. I., and M. Gurnis (2001), A low viscosity wedge in subduction zones, *Earth Planet. Sci. Lett.*, *193*, 227–236.

Billen, M. I., and G. Hirth (2007), Rheologic controls on slab dynamics, *Geochem. Geophys. Geosyst.*, *8*, Q08012, doi:10.1029/2007GC001597.

Billi, A., M. Porreca, C. Faccenna, and M. Mattei (2006), Magnetic and structural constraints for the noncylindrical evolution of a continental forebulge (Hyblea, Italy), *Tectonics*, *25*, TC3011, doi:10.1029/2005TC001800.

Bodine, J. H., M. S. Steckler, and A. B. Watts (1981), Observations of flexure and the rheology of the oceanic lithosphere, *J. Geophys. Res.*, *86*, 3695–3707.

Bott, M. H. P. (1993), Modeling the plate-driving mechanism, *J. Geol. Soc.*, *150*, 941–951.

Byerlee, J. D. (1968), Brittle-ductile transition in rocks, *J. Geophys. Res.*, *73*, 4741–4750.

Caldwell, J. G., W. F. Haxby, D. E. Karig, and D. L. Turcotte (1976), On the applicability of a universal elastic trench profile, *Earth Planet. Sci. Lett.*, *31*, 239–246.

Capitanio, F. A., G. Morra, and S. Goes (2007), Dynamic models of downgoing plate-buoyancy driven subduction: Subduction motions and energy dissipation, *Earth Planet. Sci. Lett.*, *262*, 284–297.

Cloos, M. (1993), Lithospheric buoyancy and collisional orogenesis: Subduction of oceanic plateaus, continental margins, island arcs, spreading ridges, and seamounts, *Geol. Soc. Am. Bull.*, *105*, 715–737.

Conrad, C. P., and B. H. Hager (1999), Effects of plate bending and fault strength at subduction zones on plate dynamics, *J. Geophys. Res.*, *104*, 17,551–17,571.

Davies, G. F. (1995), Penetration of plates and plumes through the mantle transition zone, *Earth Planet. Sci. Lett.*, *133*, 507–516.

Davies, G. F., and G. F. Richards (1992), Mantle convection, *J. Geol.*, *100*, 151–206.

DeMets, C., R. G. Gordon, D. F. Argus, and S. Stein (1994), Effect of recent revisions to the geomagnetic reversal time scale on estimates of current plate motions, *Geophys. Res. Lett.*, *21*(20), 2191–2194.

Enns, A., T. W. Becker, and H. Schmeling (2005), The dynamics of subduction and trench migration for viscosity stratification, *Geophys. J. Int.*, *160*, 761–775.

Faccenna, C., A. Heuret, F. Funiciello, S. Lallemand, and T. W. Becker (2007), Predicting trench and plate motion from the dynamics of a strong slab, *Earth Planet. Sci. Lett.*, *257*, 29–36.

Fukao, Y., S. Widiyantoro, and M. Obayashi (2001), Stagnant slabs in the upper and lower mantle transition region, *Rev. Geophys.*, *39*, 291–323.

Funiciello, F., C. Faccenna, D. Giardini, and K. Regenauer-Lieb (2003a), Dynamics of retreating slabs: 2. Insights from three-dimensional laboratory experiments, *J. Geophys. Res.*, *108*(B4), 2207, doi:10.1029/2001JB000896.

Funiciello, F., G. Morra, K. Regenauer-Lieb, and D. Giardini (2003b), Dynamics of retreating slabs: 1. Insights from two-dimensional numerical experiments, *J. Geophys. Res.*, *108*(B4), 2206, doi:10.1029/2001JB000898.

Funiciello, F., C. Faccenna, and D. Giardini (2004), Role of lateral mantle flow in the evolution of subduction system: Insights from 3-D laboratory experiments, *Geophys. J. Int.*, *157*, 1393–1406.

Funiciello, F., M. Moroni, C. Piromallo, C. Faccenna, A. Cenedese, and H. A. Bui (2006), Mapping mantle flow during retreating subduction: Laboratory models analyzed by feature tracking, *J. Geophys. Res.*, *111*, B03402, doi:10.1029/2005JB003792.

Garfunkel, Z., C. A. Anderson, and G. Schubert (1986), Mantle circulation and the lateral migration of subducted slabs, *J. Geophys. Res.*, *91*, 7205–7223.

Gordon, R. G., and D. M. Jurdy (1986), Cenozoic global plate motions, *J. Geophys. Res.*, *91*, 12,389–12,406.

Grevemeyer, I., N. Kaul, J. L. Diaz-Naveas, H. Villinger, C. R. Ranero, and C. Reichert (2005), Heat flow and bending-related faulting at subduction trenches: Case studies offshore of Nicaragua and central Chile, *Earth Planet. Sci. Lett.*, *236*, 238–248.

Griffiths, R. W., and J. S. Turner (1988), Folding of viscous plumes impinging on a density or viscosity interface, *Geophys. J.*, *95*, 397–419.

Gripp, A. E., and R. G. Gordon (2002), Young tracks of hotspots and current plate velocities, *Geophys. J. Int.*, *150*, 321–361.

Gurnis, M., and B. Hager (1988), Controls on the structure of subducted slab, *Nature*, *335*, 317–321.

Hager, B. H. (1984), Subducted slabs and the geoid: Constraints on mantle rheology and flow, *J. Geophys. Res.*, *89*, 6003–6015.

Heuret, A. (2005), Dynamique des zones de subduction: Etude statistique globale et approche analogique, Ph.D., Univ. Montpellier II, Montpellier, France.

Heuret, A., and S. Lallemand (2005), Plate motions, slab dynamics and back-arc deformation, *Phys. Earth Planet. Inter.*, *149*, 31–51.

Hirano, N., et al. (2006), Volcanism in response to plate flexure, *Science*, *313*, 1426–1428.

Huismans, R. S., S. J. H. Buiter, and C. Beaumont (2005), Effect of plastic-viscous layering and strain softening on mode selection during lithospheric extension, *J. Geophys. Res.*, *110*, B02406, doi:10.1029/2004JB003114.

Kanamori, H. (1994), Mechanics of earthquakes, *Annu. Rev. Earth Planet. Sci.*, *22*, 207–237.

Kincaid, C., and P. Olson (1987), An experimental study of subduction and slab migration, *J. Geophys. Res.*, *92*, 13,832–13,840.

King, S. D., and B. H. Hager (1990), The relationship between plate velocity and trench viscosity in Newtonian and power-law subduction calculations, *Geophys. Res. Lett.*, *17*, 2409–2412.

Kobayashi, K., M. Nakanishi, K. Tamaki, and Y. Ogawa (1998), Outer slope faulting associated with the western Kuril and Japan trenches, *Geophys. J. Int.*, *134*, 356–372.

Kohlstedt, D. L., B. Evans, and S. J. Mackwell (1995), Strength of the lithosphere: Constraints imposed by laboratory measurements, *J. Geophys. Res.*, *100*, 17,587–17,602.

Martinod, J., and P. Molnar (1995), Lithospheric folding in the Indian Ocean and the rheology of the oceanic plate, *Bull. Soc. Geol. Fr.*, *166*, 813–821.

Mitrovica, J. X., and A. M. Forte (1997), Radial profile of mantle viscosity: Results from the joint inversion of convection and postglacial rebound observables, *J. Geophys. Res.*, *102*, 2751–2769.

Moresi, L., and M. Gurnis (1996), Constraints on the lateral strength of slabs from three-dimensional dynamic flow models, *Earth Planet. Sci. Lett.*, *138*, 15–28.

Moresi, L., and V. Solomatov (1998), Mantle convection with a brittle lithosphere: Thoughts on the global tectonic styles of the Earth and Venus, *Geophys. J. Int.*, *133*, 669–682.

Moresi, L. N., and V. S. Solomatov (1995), Numerical investigation of 2D convection with extremely large viscosity variations, *Phys. Fluids*, *7*, 2154–2162.

Piromallo, C., T. W. Becker, F. Funiciello, and C. Faccenna (2006), Three-dimensional instantaneous mantle flow induced by subduction, *Geophys. Res. Lett.*, *33*, L08304, doi:10.1029/2005GL025390.

Ranalli, G. (1995), *Rheology of the Earth*, 413 pp., Chapman and Hall, London.

Ranero, C. R., J. P. Morgan, K. McIntosh, and C. Reichert (2003), Bending-related faulting and mantle serpentinization at the Middle America trench, *Nature*, *425*, 367–373.

Ranero, C. R., A. Villaseñor, J. Phipps Morgan, and W. Weinrebe (2005), Relationship between bend-faulting at trenches and intermediate-depth seismicity, *Geochem. Geophys. Geosyst.*, *6*, Q12002, doi:10.1029/2005GC000997.

Ribe, N. M. (2003), Periodic folding of viscous sheets, *Phys. Rev. E.*, *68*, 036305, doi:10.1103/PhysRevE.68.036305.

Ringwood, A. E., and T. Irifune (1988), Nature of the 650-km seismic discontinuity: Implications for mantle dynamics and differentiation, *Nature*, *331*, 131–136.

Schellart, W. P. (2004), Quantifying the net slab pull force as a driving mechanism for plate tectonics, *Geophys. Res. Lett.*, *31*, L07611, doi:10.1029/2004GL019528.

Schellart, W. P., J. Freeman, D. R. Stegman, L. Moresi, and D. May (2007), Evolution and diversity of subduction zones controlled by slab width, *Nature*, *446*, 308–311.

Schott, B., and H. Schmeling (1998), Delamination and detachment of a lithospheric root, *Tectonophysics*, *296*, 225–247.

Stegman, D. R., J. Freeman, W. P. Schellart, L. Moresi, and D. May (2006), Influence of trench width on subduction hinge retreat rates in 3-D models of slab rollback, *Geochem. Geophys. Geosyst.*, *7*, Q03012, doi:10.1029/2005GC001056.

Tao, W. C., and R. J. O'Connell (1993), Deformation of a weak subducted slab and variation of seismicity with depth, *Nature*, *361*, 626–628.

Turcotte, D. L., and G. Schubert (1982), *Geodynamics Application of Continuum Physics to Geological Problems*, 450 pp., John Wiley, New York.

Turcotte, D. L., D. C. McAdoo, and J. G. Caldwell (1978), An elastic-perfectly plastic analysis of the bending of the lithosphere at a trench, *Tectonophysics*, *47*, 193–205.

van Hunen, J., A. P. van den Berg, and N. J. Vlaar (2001), Latent heat effects of the major mantle phase transitions on low-angle subduction, *Earth Planet. Sci. Lett.*, *190*, 125–135.

van Hunen, J., A. P. van den Berg, and N. J. Vlaar (2002), The impact of the South-American plate motion and the Nazca Ridge

subduction on the flat subduction below South Peru, *Geophys. Res. Lett.*, *29*(14), 1690, doi:10.1029/2001GL014004.

van Keken, P. E. (2003), The structure and dynamics of the mantle wedge, *Earth Planet. Sci. Lett.*, *215*, 323–338.

van Keken, P. E., S. D. King, H. Schmeling, U. R. Christensen, D. Neumeister, and M.-P. Doin (1997), A comparison of methods for the modeling of thermochemical convection, *J. Geophys. Res.*, *102*, 22,477–22,495.

Vassiliou, M. S., and B. H. Hager (1988), Subduction zone earthquakes and stress in slabs, *Pure Appl. Geophys.*, *128*, 547–624.

Vassiliou, M. S., B. H. Hager, and A. Raefsky (1984), The distribution of earthquakes with depth and stress in subducting slabs, *J. Geodyn.*, *1*, 11–28.

Zhong, S., and M. Gurnis (1994), Controls on trench topography from dynamic models of subducted slabs, *J. Geophys. Res.*, *99*, 15,683–15,695.

Zhong, S., and M. Gurnis (1995), Mantle convection with plates and mobile, faulted plate margins, *Science*, *267*, 838–843.

Zhong, S., M. T. Zuber, L. Moresi, and M. Gurnis (2000), Role of temperature-dependent viscosity and surface plates in spherical shell models of mantle convection, *J. Geophys. Res.*, *105*, 11,063–11,082.